Atomic-Scale Morphology and Electronic Structure of Manganese Atomic Layers Underneath Epitaxial Graphene on SiC(0001)

Teng Gao,[†] Yabo Gao,[†] Cuizu Chang,[‡] Yubin Chen,[†] Mengxi Liu,[†] Shubao Xie,[†] Ke He,[‡] Xucun Ma,[‡] Yanfeng Zhang,[†,§,*] and Zhongfan Liu[†,*]

[†]Center for Nanochemistry (CNC), Beijing National Laboratory for Molecular Sciences, State Key Laboratory for Structural Chemistry of Unstable and Stable Species, College of Chemistry and Molecular Engineering, Peking University, Beijing 100871, P. R. China, [‡]Institute of Physics, Chinese Academy of Sciences, Beijing 100190, P. R. China, and [§]Department of Materials Science and Engineering, College of Engineering, Peking University, Beijing 100871, P. R. China

ABSTRACT

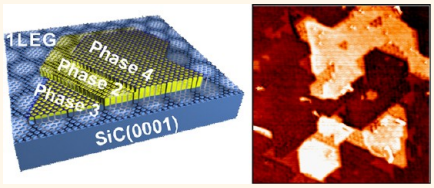

We report the fabrication of a novel epitaxial graphene(EG)/Mn/SiC(0001) sandwiched structure through the intercalation of as-deposited Mn atoms on graphene surfaces, with the aid of scanning tunneling microscope, low energy electron diffraction, and X-ray photoelectron spectroscopy. We found that Mn can intercalate below both sp^3-hybridized carbon-rich interface layer and monolayer graphene, along with the formation of various embedded Mn islands showing different surface morphologies. The unique trait of the sandwiched system is that the strong interaction between the carbon-rich interface layer and SiC(0001) can be decoupled to some degrees, and contemporaneous, an *n*-doping effect is observed by mapping the energy band of the system using angle-resolved photoemission spectroscopy. Moreover, what deserves our special attention is that the intercalated islands can only evolve below monolayer graphene when a bilayer coexists, accounting for an intriguing graphene thickness-dependent intercalation effect. In the long run, we believe that the construction of graphene/Mn/SiC(0001) systems offers ideal candidates for exploring some intriguing physical properties such as the magnetic property of two-dimensional transition metal systems.

KEYWORDS: epitaxial graphene · STM · manganese · intercalation · ARPES

Graphene, an atomic layer of graphite, possesses remarkable electronic and mechanical properties and high electron mobility and is compatible with silicon-based circuits. Graphene has attracted worldwide interest because of being a model two-dimensional prototype in condensed matter physics and having potential applications in future nanoelectronic devices.[1−3] For this goal, the quantity production of high quality graphene while simultaneously tuning its energy band is of fundamental importance. As known, except for the exfoliation method, graphene is usually prepared on some solid substrate like SiC, metal single crystals, and metal foils.[4−7] Epitaxial growth on 6H-SiC(0001) is performed through controllable sublimation of Si at high temperature, where a carbon-rich interface layer or so-called buffer layer locating between monolayer graphene and SiC substrates is inevitably formed. Along with the buffer layer is an obvious substrate-induced band-gap opening effect which reduces the transport property, such as the carrier mobility, of graphene.[7−9] Therefore, decoupling the strong interaction between the carbon lattice and the SiC(0001) substrate is essential.

In recent works, many efforts have been made on this issue using an intercalation method with noble metals of Au and Ag, alkali metal Li, and even atomic H as intercalators.[10−16] As an example, the intercalation of Au into the interface of graphene and Ni(111) and SiC(0001) can isolate graphene from its supporting substrates, through which the electronic structure can be recovered in the native free-standing state.[10,12,14] Transition metals, especially for magnetic materials such as Ni, Fe, and Mn, have a higher chemical reactivity than noble metals, which may make them perfect intercalators from the viewpoint of graphene energy band modifications and spintronics researches.[17,18] Meanwhile, the intercalated Mn layer inside the graphene system is expected to present fascinating electronic and magnetic properties different from that

* Address correspondence to yanfengzhang@pku.edu.cn, zfliu@pku.edu.cn.

Received for review December 19, 2011 and accepted August 3, 2012.

Published online August 03, 2012
10.1021/nn302303n

of bulk Mn, considering the quantum confinement effect. Recall that thin Mn films and their interfaces with semiconductor substrates have demonstrated wide applications in spintronics, in which they were ordinarily grown on single crystal surfaces under ultrahigh vacuum conditions in order to avoid oxidations.[19−24] Even so, measurements of UHV prepared Mn systems are still challenging for the necessity of transferring samples out of the vacuum chamber. In this case, fabricating thin Mn films stable at ambient conditions and compatible with traditional transport measurement techniques, is a key issue for future nanodevice applications. According to a recent report, graphene can act as coating layers for locking water adlayers above mica.[25] Similarly, graphene can serve as coating layer for intercalated metal layers to prevent oxidation, if some specific metal−graphene intercalation system can be established.

In this work, we focused on the intercalation of transition-metal Mn into epitaxial graphene on SiC(0001), and characterized the intercalation nature by virtue of some surface sensitive analytical methods such as scanning tunneling microscopy (STM), low energy electron diffraction (LEED), X-ray photoelectron spectroscopy (XPS) and angle-resolved photoemission spectroscopy (ARPES). Step-wise thermal annealing under high vacuum conditions is designed to serve as driving forces for the intercalation process. On one hand, we expect that the carbon-rich interface layer strongly affecting the transport properties of epitaxial graphene can be partially decoupled form the substrate by Mn intercalation. On the other hand, we anticipate that Mn atomic layers underneath inert graphene systems can be constructed for future novel property explorations. By varying the deposition amount of Mn onto the few layer coexisting graphene, the intercalation mechanism is expected to be revealed using systematic experimental proofs.

RESULTS AND DISSCUSSION

Epitaxial growth of graphene on SiC(0001) substrates usually leads to coexisting few layer graphene, while through controlling the sublimation temperature and time, the thicknesses of epitaxial graphene (EG) can be controlled to be monolayer or bilayers as characterized by STM and LEED.[26] However, the substrate of few-layer coexisting graphene is helpful for investigating the nucleation of metal clusters after evaporation, as well as the immigration of metal atoms upon thermal annealing as a function of graphene thickness, and hereby a thickness-dependent surface property.[10,12,14,15]

In this research, it is not so exceptional to see that, after thermal evaporation, Ni and Mn atoms evolve into nanoclusters on the graphene substrate at room temperature. Interestingly, after stepwise annealing to 800 °C, the incomplete bilayer graphene was cut into

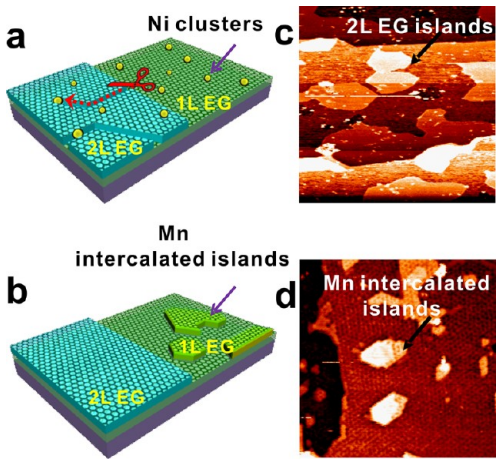

Figure 1. (a and b) Schematic maps illustrating the cutting of incomplete bilayer epitaixal graphene (EG) by Ni clusters and the intercalation of Mn into EG/SiC(0001) through thermal annealing treatments. (c) (−0.45 V, 1.00 nA) and (d) (−0.007 V, 1.76 nA) (100 nm ×100 nm) corresponding STM morphologies of panels a and b.

separate hexagonal graphene patches, as illustrated in the schematic image in Figure 1a and in the corresponding STM result in Figure 1c for the Ni/EG/SiC(0001) system. The as-deposited Ni clusters are proposed to serve as scissors in the cutting process. Similar results were reported that mechanically exfoliating graphene can be etched by Ni, Fe, and Co nanoparticles through a hydrogenation catalysis mechanism.[27,28] Considering there is no hydrogen in the UHV chamber, a different mechanism should play for the current system. Noting the relative high solubility of C into Ni (2.7%),[29] sequential processes should occur, including (1) annealing induced diffusion of Ni clusters along specific directions mediated by substrate symmetries; (2) dissolution of C into Ni; (3) desorption of Ni along with the rearrangement of C atoms or transformation of bigger graphene flakes into smaller ones. In this case, the dissolution of carbon into Ni clusters and the following desorption of Ni throughout the thermal annealing treatment should be the potential mechanism for the etching behavior. Otherwise, it is worthy of noting that atomically resolved STM images on the boundaries of the hexagonal patches usually show a perfect armchair-type structure, accounting for a directional cutting behavior probably induced by the substrate lattice symmetry effect.

In contrary to Ni, after annealing at ∼600 °C, Mn clusters vanish on graphene surfaces with the appearance of polygonal islands on thinner graphene, as shown in Figure 1b and Figure 1d. A different reaction mechanism is expected for Mn on epitaxial graphene with regard to Ni, while this phenomenon has not been reported before.

To achieve a deeper understanding of the reaction mechanism, various amounts of Mn were deposited onto the carbon-rich interface layer, followed with annealing at 600 °C for 30 min. After a 0.1 ML Mn

intercalation, polygonal Mn islands were observed on the carbon-rich interface layer (Figure 2a). With increasing Mn deposition to 0.3 ML, more Mn islands were formed, with some of them located on the rarely appearing monolayer graphene (Figure 2b). Interestingly, detailed STM characterization (Figure 2c) revealed that Mn islands on the interface layer had a uniform height of ~300 pm, in accord with the height of a single layer of Mn. Moreover, these Mn islands had a flatter surface (roughness, ~50 pm) than that of the surrounding interface layer (roughness, ~120 pm). Additionally, typical graphene lattices were observed on these Mn deposition-induced islands by atomic resolution STM images (Figure 2d). All these facts proved that Mn atoms were intercalated below the interface layer. Accordingly, the carbon-rich interface layer was partially decoupled from the Si-terminated SiC(0001) substrate by the Mn intercalation, leading to nearly free-standing graphene flakes over the Mn islands. This phenomenon is illustrated by schematic diagrams (Figures 2e,f).

As mentioned above, the Mn intercalated islands on monolayer graphene (Figure 2b) exhibited different morphologies or contrasts, compared to the formation of islands with unique contrasts on the carbon-rich interface layer. Detailed experiments with alternations of annealing temperature and time were performed to the monolayer graphene/interface layer/SiC(0001) system. Figure 3a shows polygonal islands upon 300 °C annealing of Mn clusters on a substrate mainly composed of monolayer graphene. The line-profile extracted along the dashed line in Figure 3a reveals an average apparent height of ~290 pm for the three islands in the middle terrace of SiC(0001). This height seems to be comparable with the atomic layer height of Mn but much lower than that of graphene (~340 pm), probably illustrating a Mn atomic layer over epitaxial graphene configuration.[19] In the context, this structure is defined as phase 1. Another special feature is that above the island surface, no honeycomb lattice typical for monolayer graphene can be observed, which provides side evidence for Mn layer locating on monolayer graphene (in parallel with phase 1).

After the sample was subsequently annealed at 600 °C for 10 min, the polygonal islands corresponding to phase 1 evolved into two types of islands which are differentiated as phases 2 and 4 by their different apparent heights of ~340 pm and ~450 pm, as exemplified in Figure 3b. Above phase 2, the same $(6\sqrt{3} \times 6\sqrt{3})R30°$ reconstruction as that of the carbon-rich interface layer can be noticed, while this does not happen on phase 4. In addition, it is clear to see that both phases usually coexist inside a single island, as shown in the upper left part of Figure 3b. For the two-phase mixed island, there are two points worthy of noting: first, the island seems much more compact with their peripheries oriented by a multiple of 60°

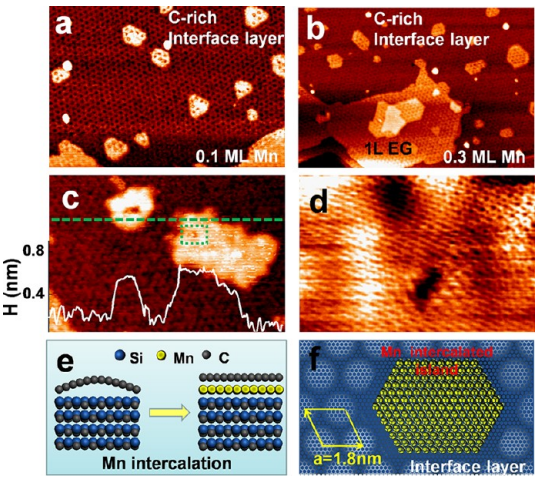

Figure 2. (a) (−1.71 V, 1.09 nA) (100 nm × 68 nm) and (b) (−1.85 V, 1.09 nA) (145 nm ×100 nm) STM morphologies of 0.1 and 0.3 ML Mn intercalation below the carbon-rich interface layer, respectively. (c) (−0.025 V, 1.82 nA) (67 nm × 44 nm) Zoom-in view of the Mn intercalated islands. The line-profile along the dashed line presents the flat islands having an apparent height of ~300 pm. (d) (−0.025 V, 1.82 nA) (11 nm × 5 nm) Atomic-resolution STM image on the square in panel c showing graphene lattices above the intercalated island. (e and f) Side-view and top-view models of Mn intercalation below the carbon-rich interface layer.

which illustrates a strong substrate symmetry effect. Second, a preferential phase transition from the island boundary is observed in Figure 3b, where phase 2 evolves at the periphery of the island of phase 1. These features may provide side evidence that kinetic and thermodynamic processes are both acting as driving forces.[26,30]

Through further annealing at 600 °C, the surface phase uniformity is greatly enhanced (Figure 3c), with 80% of Mn deposition induced islands changing into phase 4 and the other 20% into phase 2. Meanwhile, a new phase presenting an apparent height of 120 pm (phase 3) appears with no $(6\sqrt{3} \times 6\sqrt{3})R30°$ modulation showing on island surfaces. Of particular significance is that when annealing at 900 °C, the multilayered islands begin to shrink into smaller compact ones, due to the thermal desorption of Mn (see Supporting Information, Figure 1S). The extra stability of Mn islands, that is, far beyond its thermal deposition temperature, addresses that Mn atoms were intercalated below monolayer graphene which partially prevented Mn from being desorbed.

As discussed above, in order to get a clear picture of Mn-induced islands in various phases, apparent height and surface morphologies were carefully characterized. On the basis of these results, a schematic diagram is tentatively summarized in Figure 3d for phases 2−4. According to the experimental results, a schematic diagram is also provided in Figure 3e to illustrate the probable channels for Mn intercalation. For phase 1, one atomic layer of Mn is proposed to inhabit over monolayer graphene. With thermal annealing, Mn atoms

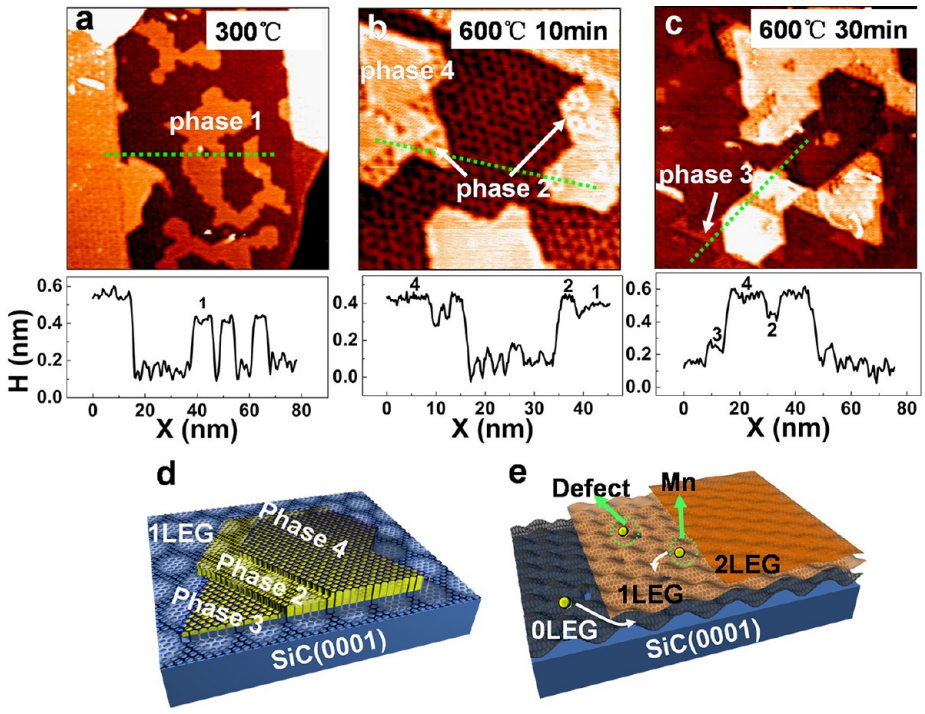

Figure 3. STM images showing the morphologies of Mn deposition induced islands *via* (a) (−1.45 V, 1.10 nA) (100 nm × 100 nm) annealing at 300 °C for 10 min, (b) (−0.009 V, 1.00 nA) (50 nm × 50 nm) 600 °C, 10 min, (c) (−0.008 V, 1.00 nA) (100 nm × 100 nm) 600 °C, 30 min. Section views along the lines in (a−c) present various apparent heights for phase 1 of ∼290 pm, phase 2 of ∼340 pm, phase 3 of ∼120 pm, and phase 4 of ∼450 pm, respectively. The schematic diagram in panel d illustrates different surface morphologies and apparent heights of Mn islands in phases 2, 3, and 4, with intercalation channels demonstrated in panel e.

are activated to a high energy state enough to overcome some energy barriers to be trapped below monolayer graphene. However, as reported before, a perfect graphene sheet is impermeable to gas molecules (even for small helium molecules) since the substantial electron density of the aromatic carbon rings create a giant barrier for atoms and molecules in passing through graphene sheet.[31,32] Comparatively, Mn atoms, having a bigger radius than helium molecules, should not be able to penetrate directly through the graphene lattice. In contrast, intercalation starting from the defect sites or step boundaries was reported in recent works with Ni, Fe, Co as intercalators.[16,18,33] For Mn intercalation into the epitaxial graphene system, a similar mechanism was proposed because the defect sites really appear under some scanning conditions (see Figure 2S).

Although the experimental facts can be preliminarily explained by large-scale STM examinations and their height-profile analysis, more confirmative results are still highly needed. First, in Figure 4a,b, an atomic-scale image of the Mn-deposition induced island (marked as phase 4) is captured, where a perfect continuity of carbon lattice over both monolayer graphene in the right part of Figure 4b and the hexagonal island in the left part can be noticed. This provides side evidence that the Mn-deposition induced island is actually formed by intercalation of Mn below the graphene layer.

Second, the quantum interference effect is frequently obtained at the island edge which provides additional clue that the in-plane flatness of graphene can be perturbed by the underneath island (Figure 4c). This is clearly observed in the zoom-in image of Figure 4d showing a typical $(\sqrt{3} \times \sqrt{3})R30°$ interference pattern, and again convinced by its 2D FFT pattern inserted in Figure 4d. According to published literatures, this quantum interference usually occurs near the edge of graphene due to electron scattering effects.[34−36]

Third, LEED patterns of the same monolayer graphene sample before and after Mn intercalation were recorded in Figure 4 panels e and f, respectively. The intercalated sample is mainly composed of phase 3 and phase 4 (dominating 30% of the surface), prepared through annealing as-deposited Mn (0.5 ML) for 30 min. It is known that the satellite spots around graphene (1 × 1) spots originate from the reconstructed $(6\sqrt{3} \times 6\sqrt{3})R30°$ interface layer. Interestingly, after Mn intercalation, it is found that the superstructure spots were obviously suppressed. This indicates that the carbon-rich interface layer is partially decoupled from the substrate through the intercalation process.[13] (see more discussions in Supporting Information, Figure 3S)

What merits our special interest is that graphene can act as protection layers of Mn films intercalated into epitaxial graphene over SiC(0001) in order to avoid oxidations. This was proven by transferring the sample out of the vacuum chamber, keeping at the atmosphere

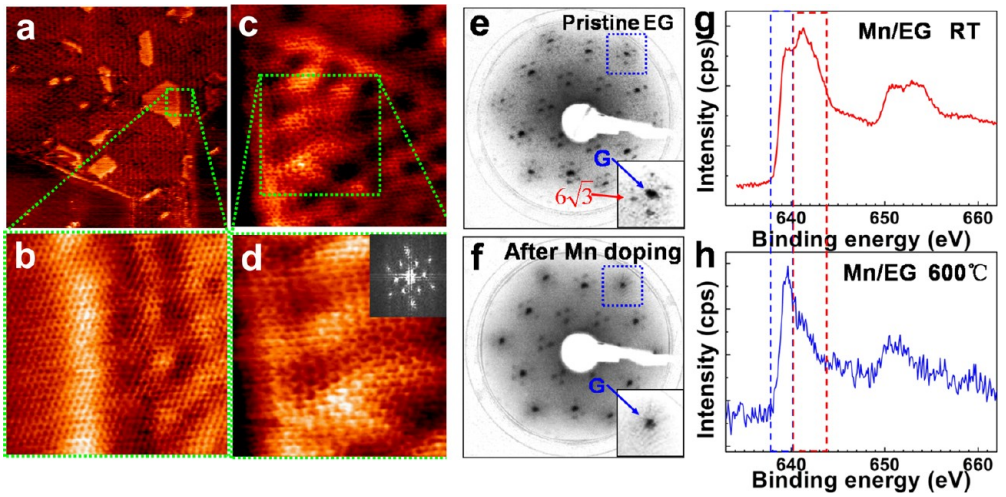

Figure 4. (a) (−0.002 V, 1.20 nA) (100 nm × 100 nm) STM image of Mn-deposition induced islands. (b) (−0.002 V, 1.20 nA) (10 nm × 10 nm) Atomic-scale image over the island boundary showing a perfect continuity of graphene. (c) (−0.05 V, 1.00 nA) (15 nm × 15 nm) and (d) (−0.054 V, 1.00 nA) (7 nm × 7 nm) Clear quantum interference phenomenon over an island surface evidenced by the ($\sqrt{3} \times \sqrt{3}$)*R*30° reconstructed lattice and its 2D FFT map. (e, f) LEED patterns of monolayer graphene before and after Mn intercalation. (g, h) XPS spectra of Mn clusters and Mn deposition induced islands on SiC(0001) captured after a long-time exposure of the samples to atmospheric conditions.

for several days, and then performing XPS measurements. It is known that the sharp peak around 639 eV is special for Mn 2p core-level and thus can be regarded as the token of metal state Mn, and the peaks with binding energies ranging from 641 to 643 eV correspond to the oxidized states of Mn. In Figure 4g, after Mn deposition at room temperature prior to thermal annealing, the samples can be easily oxidized by O_2 under atmospheric conditions, which are addressed by the appearance of the broad peak around 642 eV. On the contrary, another sample was annealed in an UHV chamber at 600 °C after Mn deposition, and a sharp peak locating at 639 eV (Figure 4h) appeared to be in line with the intercalated Mn layers. In view of this, the XPS data can also support credible evidence of the intercalation behavior when the as-deposited Mn clusters on SiC(0001) are heated to above 600 °C (see more discussions in Supporting Information with Figure 4S).

For the Mn intercalated system, it is intriguing to know if the intercalation process can modify the energy band of epitaxial graphene. This issue can be resolved by mapping the density of electron states along $\overline{\Gamma—K}$ direction in momentum space using ARPES. In Figure 5a, the energy band of epitaxial graphene was recorded to show a linear shape around the Dirac point which is the characteristics of monolayer graphene. After 0.1 ML Mn intercalation, the Dirac point shifts down by ∼30 meV from the Fermi energy (Figure 5b), indicating an obvious *n*-doping effect. And the Dirac cone vanishes when the Mn coverage reaches 0.6 ML (Figure 5c). On one hand, this can be explained from the perturbation of 3d electronic states of Mn (locating very close to the Fermi level) on the linear energy band of graphene at a relative high Mn coverage.[37] That is, the linear energy band of graphene

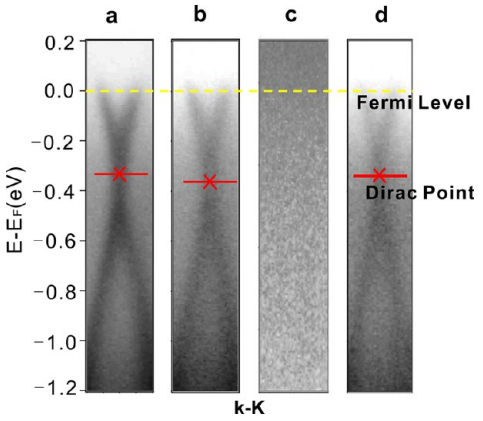

Figure 5. (a) Electronic structure of epitaxial graphene along $\overline{\Gamma—K}$ with a linear energy dispersion around the Dirac point indicated with crossings, (b) after 0.1 ML Mn intercalation; (c) after 0.6 ML Mn intercalation; (d) Recovering of graphene energy band by heating sample c up to 1200 °C.

is smeared out with Mn deposition. On the other hand, the native energy band of graphene can also be weakened with the Mn intercalation process, because of the reduction of the intact graphene regions. Interestingly, after sample heating to 1200 °C for a short time, the Dirac cone can be renewed to be the native state, in parallel with the desorption of Mn (Figure 5d). To summarize the data, moderate Mn intercalations can cause reversible *n*-doping of epitaxial graphene, while unfortunately the pristine energy band cannot be intensively modified.

It is fascinating to know if, with an increase in Mn intercalation, the density of intercalated Mn islands depends strictly on the thickness of the underlying graphene. To clarify this issue, a systematic experiment was executed on SiC samples, mainly covered by

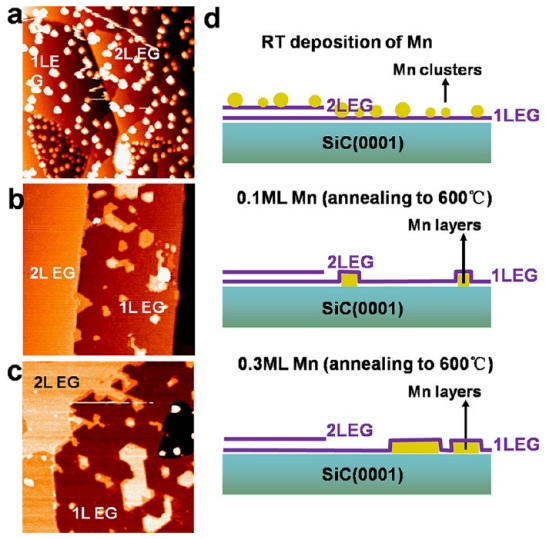

Figure 6. (a) (−0.12 V, 0.37 nA) (150 nm × 150 nm) STM morphology after Mn deposition on mono- and bilayer coexisting graphene with the formation of Mn nanoclusters. (b) (−0.05 V, 1.06 nA) (150 nm × 150 nm) Preferred intercalation of Mn into 1 L EG at 0.1 ML Mn deposition through annealing the sample to 600 °C. (c) (−0.02 V, 1.00 nA) (216 nm × 216 nm) Increased intercalation into 1 L EG regions at 0.3 ML Mn deposition and annealing. (d) Schematic-views showing the graphene thickness-dependent intercalation behavior.

mono- and bilayer graphene. The STM morphology in Figure 6a presents the formation of nanoclusters after Mn deposition on the room temperature SiC(0001) substrate. Upon the sample being annealed to 600 °C, Mn clusters evolve into intercalated Mn islands which preferentially reside in monolayer regions or terraces, as exemplified in Figure 6b. With a further increase in the deposition amounts of Mn, the individual islands are gradually connected together to show fractional shapes. And in this process, almost no island formation can be noticed in the bilayer region (Figure 6c). For the possible reasons of the preferred nucleation, the Bernal stacking geometry of bilayer graphene, as well as the intercalation barriers for mono- and bi-regions should be considered. For the former case, as mentioned above, the intercalation channels of Mn into graphene is proposed to be graphene boundaries and defects sites, since the size of the hexagonal hole of the graphene lattice is much smaller than the diameter of a metal ion such as Mn, hence penetration of Mn directly from both sides of the carbon network is not practical. For the latter case, it is not so hard to imagine that the intercalation of Mn into monolayer epitaxial graphene/SiC(0001) should be generated by sequential penetration through the monolayer graphene, carbon rich interface layer, and finally arrival at the Si-faceted substrate; Mn residing between the interface layer and substrate should be in a stable state, which can also be supported from the former results about the preferential intercalation of Mn into the interface layer rather than the monolayer graphene depicted in Figure 3. However, for the bilayer intercalation, Mn atoms need to penetrate one more graphene layer to reach the most stable state, and this process should be inhibited when the monolayer graphene region still exists. In essence, the chemical bonding formation between Si and Mn is expected to serve as the fundamental driving forces for the intercalation process, although different graphene layers present various intercalation barriers. Note that further theoretical calculation is still desirable in the interest of achieving a deeper understanding of the observed thickness-dependent penetration behavior.

CONCLUSION

In this work, we constructed a novel monolayer graphene/Mn/SiC(0001) sandwiched structure and characterized its morphology and electronic properties using STM, LEED, and XPS. A key finding is that on few-layer coexisting graphene, Mn atoms can only intercalate into a carbon-rich interface layer and monolayer regions through a stepwise thermal annealing process, hereby showing a strong graphene thickness dependence effect. Owing to the existing carbon-rich interface layer between monolayer graphene and SiC(0001), Mn layers can stay below monolayer graphene or/and below the carbon-rich interface layer with the formation of various phases presenting different STM morphologies. Through this intercalation process, partial decoupling of the interface layer from Si-terminated SiC(0001) can be automatically realized. Of particular importance is that a lowering of the Dirac point in parallel with an *n*-doping effect was only observed on the graphene samples with a small amount Mn intercalation by mapping the energy band using ARPES. In addition, it is worth noting that the two-dimensional Mn layers intercalated into a graphene/SiC-(0001) system can be free of oxidations, which makes an Mn layer the perfect prototype for exploring some intriguing physical properties such as the magnetic property of low dimensional systems.

METHODS

Preparation of Sample. An *n*-doped 6H-SiC(0001) with carrier density of 10^{16} cm^{-3} was used as the substrate for graphene growth inside the ultrahigh vacuum condition. It was first degassed at 850 °C for 60 min (without exposure to silicon flux), and then annealed to 1400 °C for a few minutes for graphene growth.[7] The depositions of Ni and Mn were carried out in a molecular beam epitaxy (MBE) chamber with the evaporation rate recorded by an *in situ* thickness monitor at a maximum flux of 0.5 Å/min. After metal deposition, the sample was annealed under 300, 600, and 900 °C by a direct current heating mode in order to realize intercalations of metal clusters.

STM, LEED, XPS, and ARPES Characterizations. The morphologies of samples were characterized by high-resolution STM and LEED equipped in a vacuum chamber with a base pressure better than 1×10^{-10} mbar. Contemporaneous, the Mn decorated graphene samples before and after thermal annealing treatments were also transferred out of the vacuum chamber for identification of the bonding configuration of Mn by virtue of XPS. In ARPES measurements, photoelectrons are excited by an unpolarized He−Iα light (21.21 eV) and collected by a Scienta SES-2002 analyzer (15 meV).

Conflict of Interest: The authors declare no competing financial interest.

Acknowledgment. This work was financially supported by the Ministry of Science and Technology of China (Grants Nos. 2012CB921404, 2011CB921903) and the National Natural Science Foundation of China (Grants Nos. 21073003).

Supporting Information Available: Additional supporting STM figures. This material is available free of charge *via* the Internet at http://pubs.acs.org.

REFERENCES AND NOTES

1. Novoselov, K. S.; Geim, A. K.; Morozov, S. V.; Jiang, D.; Zhang, Y.; Dubonos, S. V.; Grigorieva, I. V.; Firsov, A. A. Electric Field Effect in Atomically Thin Carbon Films. *Science* **2004**, *306*, 666–669.
2. Novoselov, K. S.; Geim, A. K.; Morozov, S. V.; Jiang, D.; Katsnelson, M. I.; Grigorieva, I. V.; Dubonos, S. V.; Firsov, A. A. Two-dimensional Gas of Massless Dirac Fermions in Graphene. *Nature* **2005**, *438*, 197–200.
3. Zhang, Y.; Tan, Y.-W.; Stormer, H. L.; Kim, P. Experimental Observation of the Quantum Hall Effect and Berry's Phase in Graphene. *Nature* **2005**, *438*, 201–204.
4. Marchini, S.; Gunther, S.; Wintterlin, J. Scanning Tunneling Microscopy of Graphene on Ru(0001). *Phys. Rev. B* **2007**, *76*, 075429.
5. Li, X.; Cai, W.; An, J.; Kim, S.; Nah, J.; Yang, D.; Piner, R.; Velamakanni, A.; Jung, I.; Ruoff, R. S.; *et al.* Large-Area Synthesis of High-Quality and Uniform Graphene Films on Copper Foils. *Science* **2009**, *324*, 1312–1314.
6. Wintterlin, J.; Bocquet, M. L. Graphene on Metal Surfaces. *Surf. Sci.* **2009**, *603*, 1841–1852.
7. Emtsev, K. V.; Bostwick, A.; Horn, K.; Jobst, J.; Kellogg, G. L.; Ley, L.; McChesney, J. L.; Ohta, T.; Reshanov, S. A.; Seyller, T.; *et al.* Towards Wafer-Size Graphene Layers by Atmospheric Pressure Graphitization of Silicon Carbide. *Nat. Mater.* **2009**, *8*, 203–207.
8. Bolotin, K. I.; Sikes, K. J.; Jiang, Z.; Klima, M.; Fudenberg, G.; Hone, J.; Kim, P.; Stormer, H. L. Ultrahigh Electron Mobility in Suspended Graphene. *Solid State Commun.* **2008**, *146*, 351–355.
9. Shivaraman, S.; Barton, R. A.; Yu, X.; Alden, J.; Herman, L.; Chandrashekhar, M. V. S.; Park, J.; McEuen, P. L.; Craighead, H. G.; Spencer, M. G.; *et al.* Free-Standing Epitaxial Graphene. *Nano Lett.* **2009**, *9*, 3100–3105.
10. Varykhalov, A.; Sanchez-Barriga, J.; Shikin, A. M.; Biswas, C.; Vescovo, E.; Rybkin, A.; Marchenko, D.; Rader, O. Electronic and Magnetic Properties of Quasifreestanding Graphene on Ni. *Phys. Rev. Lett.* **2008**, *101*, 157601.
11. Choi, S. M.; Jhi, S. H. Electronic Property of Na-Doped Epitaxial Graphenes on SiC. *Appl. Phys. Lett.* **2009**, *94*, 153108.
12. Premlal, B.; Cranney, M.; Vonau, F.; Aubel, D.; Casterman, D.; De Souza, M. M.; Simon, L. Surface Intercalation of Gold Underneath a Graphene Monolayer on SiC(0001) Studied by Scanning Tunneling Microscopy and Spectroscopy. *Appl. Phys. Lett.* **2009**, *94*, 263115.
13. Riedl, C.; Coletti, C.; Iwasaki, T.; Zakharov, A. A.; Starke, U. Quasi-Free-Standing Epitaxial Graphene on SiC Obtained by Hydrogen Intercalation. *Phys. Rev. Lett.* **2009**, *103*, 246804.
14. Gierz, I.; Suzuki, T.; Weitz, R. T.; Lee, D. S.; Krauss, B.; Riedl, C.; Starke, U.; Hochst, H.; Smet, J. H.; Kern, K.; *et al.* Electronic Decoupling of an Epitaxial Graphene Monolayer by Gold Intercalation. *Phys. Rev. B* **2010**, *81*, 235408.
15. Virojanadara, C.; Watcharinyanon, S.; Zakharov, A. A.; Johansson, L. I. Epitaxial graphene on 6*H*-SiC and Li intercalation. *Phys. Rev. B* **2010**, *82*, 205402.
16. Li, Y.; Zhou, G.; Li, J.; Wu, J.; Gu, B.-L.; Duan, W. Lithium Intercalation Induced Decoupling of Epitaxial Graphene on SiC(0001): Electronic Property and Dynamic Process. *J. Phys. Chem. C* **2011**, *115*, 23992–23997.
17. Jayasekera, T.; Kong, B. D.; Kim, K. W.; Buongiorno Nardelli, M. Band Engineering and Magnetic Doping of Epitaxial Graphene on SiC (0001). *Phys. Rev. Lett.* **2010**, *104*, 146801.
18. Sicot, M.; Leicht, P.; Zusan, A.; Bouvron, S.; Zander, O.; Weser, M.; Dedkov, Y. S.; Horn, K.; Fonin, M. Size-Selected Epitaxial Nanoislands Underneath Graphene Moiré on Rh(111). *ACS Nano* **2012**, *6*, 151–158.
19. Wu, H.; Hortamani, M.; Kratzer, P.; Scheffler, M. First-Principles Study of Ferromagnetism in Epitaxial Si−Mn Thin Films on Si(001). *Phys. Rev. Lett.* **2004**, *92*, 237202.
20. Yamada, T. K.; Bischoff, M. M. J.; Mizoguchi, T.; van Kempen, H. STM and STS Study of Ultrathin Mn Layers on Fe(001). *Surf. Sci.* **2002**, *516*, 179–190.
21. Flores, T.; Hansen, M.; Wuttig, M. Structure and growth of Mn on Cu(100). *Surf. Sci.* **1992**, *279*, 251–264.
22. Kim, S. K.; Tian, Y.; Montesano, M.; Jona, F.; Marcus, P. M. Simple Structure and Soft Elastic Behavior of Mn on Fe{001}. *Phys. Rev. B* **1996**, *54*, 5081–5085.
23. Pfandzelter, R.; Igel, T.; Winter, H. Growth and Structure of Ultrathin Mn Films on Fe(001). *Surf. Sci.* **1997**, *389*, 317–328.
24. Schneider, J.; Rosenhahn, A.; Wandelt, K. STM Measurements on Alloy Formation During Submonolayer Growth of Mn on Cu(111). *Appl. Surf. Sci.* **1999**, *142*, 68–74.
25. Xu, K.; Cao, P. G.; Heath, J. R. Graphene Visualizes the First Water Adlayers on Mica at Ambient Conditions. *Science* **2010**, *329*, 1188–1191.
26. Emtsev, K. V.; Speck, F.; Seyller, T.; Ley, L.; Riley, J. D. Interaction, Growth, and Ordering of Epitaxial Graphene on SiC{0001} Surfaces: A Comparative Photoelectron Spectroscopy Study. *Phys. Rev. B* **2008**, *77*, 155303.
27. Campos, L. C.; Manfrinato, V. R.; Sanchez-Yamagishi, J. D.; Kong, J.; Jarillo-Herrero, P. Anisotropic Etching and Nanoribbon Formation in Single-Layer Graphene. *Nano Lett.* **2009**, *9*, 2600–2604.
28. Ci, L.; Xu, Z.; Wang, L.; Gao, W.; Ding, F.; Kelly, K.; Yakobson, B.; Ajayan, P. Controlled Nanocutting of Graphene. *Nano Res.* **2008**, *1*, 116–122.
29. Liu, N.; Fu, L.; Dai, B.; Yan, K.; Liu, X.; Zhao, R.; Zhang, Y.; Liu, Z. Universal Segregation Growth Approach to Wafer-Size Graphene from Non-noble Metals. *Nano Lett.* **2010**, *11*, 297–303.
30. Poon, S. W.; Chen, W.; Wee, A. T. S.; Tok, E. S. Growth Dynamics and Kinetics of Monolayer and Multilayer Graphene on a 6H-SiC(0001) Substrate. *Phys. Chem. Chem. Phys.* **2010**, *12*, 13522–13533.
31. Bunch, J. S.; Verbridge, S. S.; Alden, J. S.; van der Zande, A. M.; Parpia, J. M.; Craighead, H. G.; McEuen, P. L. Impermeable Atomic Membranes from Graphene Sheets. *Nano Lett.* **2008**, *8*, 2458–2462.
32. Jiang, D.-e.; Cooper, V. R.; Dai, S. Porous Graphene as the Ultimate Membrane for Gas Separation. *Nano Lett.* **2009**, *9*, 4019–4024.
33. Boukhvalov, D. W.; Katsnelson, M. I. Destruction of Graphene by Metal Adatoms. *Appl. Phys. Lett.* **2009**, *95*, 023109.
34. Yang, H.; Mayne, A. J.; Boucherit, M.; Comtet, G.; Dujardin, G.; Kuk, Y. Quantum Interference Channeling at Graphene Edges. *Nano Lett.* **2010**, *10*, 943–947.
35. Zhang, Y.; Brar, V. W.; Wang, F.; Girit, C.; Yayon, Y.; Panlasigui, M.; Zettl, A.; Crommie, M. F. Giant Phonon-Induced Conductance in Scanning Tunnelling Spectroscopy of Gate-Tunable Graphene. *Nat. Phys.* **2008**, *4*, 627–630.
36. Rutter, G. M.; Crain, J. N.; Guisinger, N. P.; Li, T.; First, P. N.; Stroscio, J. A. Scattering and Interference in Epitaxial Graphene. *Science* **2007**, *317*, 219–222.
37. Jeong, T. Magnetic Properties of Mn_3Si from First-Principles Studies. *Phys. B: Condens. Matter* **2012**, *407*, 888–890.